arXiv:1401.5923v1 [nlin.CD] 23 Jan 2014

Temporal flooding of regular islands by chaotic wave packets

Lars Bittrich[1,2], Arnd Bäcker[1,2], and Roland Ketzmerick[1,2]
[1] *Technische Universität Dresden, Institut für Theoretische Physik and Center for Dynamics, 01062 Dresden, Germany*
[2] *Max-Planck-Institut für Physik komplexer Systeme, Nöthnitzer Straße 38, 01187 Dresden, Germany*
(Dated: 22.01.2014)

We investigate the time evolution of wave packets in systems with a mixed phase space where regular islands and chaotic motion coexist. For wave packets started in the chaotic sea on average the weight on a quantized torus of the regular island increases due to dynamical tunneling. This flooding weight initially increases linearly and saturates to a value which varies from torus to torus. We demonstrate for the asymptotic flooding weight universal scaling with an effective tunneling coupling for quantum maps and the mushroom billiard. This universality is reproduced by a suitable random matrix model.

PACS numbers: 05.45.Mt, 03.65.Sq

I. INTRODUCTION

Typical Hamiltonian systems have a mixed phase space in which dynamically separated regular and chaotic regions coexist. A fundamental question is how the properties of the classical dynamics are reflected in the corresponding quantum system [1, 2]. In the semiclassical limit, i.e. at short wave length or when typical actions become large in comparison to Planck's constant, one expects according to the semiclassical eigenfunction hypothesis that eigenstates localize on classically invariant regions in phase space [3–5]. Thus they can be classified as regular or chaotic, see e. g. [6–11]. Away from the semiclassical limit, however, the correspondence between eigenstates and classically invariant regions breaks down. For example partial barriers can lead to localization of eigenstates and wave packets [6, 12–16]. Another phenomenon is dynamical tunneling [17, 18] between regular and chaotic phase-space regions. As a consequence regular states only exist if in addition to the WKB-quantization condition the relation [19, 20]

$$\gamma_m < \frac{1}{\tau_{\mathrm{H,ch}}} \tag{1}$$

is fulfilled, where γ_m is the regular-to-chaotic tunneling rate from the mth torus to the chaotic sea and $\tau_{\mathrm{H,ch}} = h_{\mathrm{eff}}/\Delta_{\mathrm{ch}}$ is the Heisenberg time of the chaotic sea with mean level spacing Δ_{ch}. If the criterion (1) is violated the mth regular state disappears and the corresponding region in phase space is flooded by chaotic states. The transition region, until the state fully disappears, is rather broad. An important consequence are huge localization lengths in nano wires with surface disorder [21, 22]. Also eigenstates in higher-dimensional systems are influenced by flooding [23].

Flooding also occurs in the time evolution of wave packets. Starting a wave packet in the chaotic sea it will partially or completely flood the regular island [19], see Fig. 1. The determination of tunneling rates γ_m entering in Eq. (1) has been studied in much detail, see e.g. [18, 24, 25], including consequences on spectral statistics [26], quality factors in optical microcavities [27], and the existence of bouncing-ball modes [28].

In this paper we study this temporal flooding of the regular island not just for the entire regular island [19], but specifically for individual tori. We quantify the amount of flooding of a torus by a suitably defined weight. This flooding weight initially increases linearly. At a saturation time it reaches its asymptotic value. We observe that the asymptotic flooding weight and the saturation time for individual tori show a universal scaling with an effective tunneling coupling. This is found for a suitably designed quantum map as well as the generic standard map and the mushroom billiard. The universality is reproduced by an appropriate random matrix model.

This paper is organized as follows: Temporal flooding is introduced for the designed quantum map in Sec. II. The initial linear increase of the flooding weight is explained in Sec. III. The following Sec. IV deals with the universal scaling of the asymptotic flooding weight and its modelling by random matrices. Further applications to the standard map and the mushroom billiard are presented in Sec. V. A summary and outlook is given in Sec. VI.

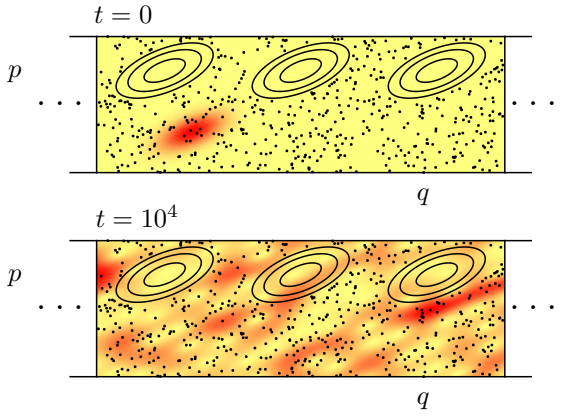

FIG. 1. (Color online) Flooding in a system with a mixed phase space. A wave packet started at $t = 0$ in the chaotic sea (dots) floods the regular island (closed lines) for large times.

II. TEMPORAL FLOODING

A. System

For the study of temporal flooding in a mixed phase space we consider an example system with one large regular island surrounded by a chaotic sea [20, 29]. This is realized by a kicked Hamiltonian system

$$H(p,q,t) = T(p) + V(q) \sum_{n=-\infty}^{\infty} \delta(t-n) \ , \qquad (2)$$

where the potential $V(q)$ and the kinetic energy $T(p)$ are designed appropriately with periodic boundary conditions in q- and p-direction, see Appendix A for a detailed definition. One considers the dynamics stroboscopically just after each kick, giving an area preserving designed map, see Fig. 2(a).

Quantum mechanically the dynamics of such a map is described by a unitary operator U (see e.g. [30–33])

$$U = \exp\left(-\frac{2\pi \mathrm{i}}{h_{\mathrm{eff}}} V(q)\right) \exp\left(-\frac{2\pi \mathrm{i}}{h_{\mathrm{eff}}} T(p)\right) \ , \qquad (3)$$

which determines the time evolution of wave packets

$$|\varphi_t\rangle = U^t \, |\varphi_0\rangle \ , \ t = 0, 1, 2, \ldots \ . \qquad (4)$$

The dimension of the Hilbert space is given by $N = 1/h_{\mathrm{eff}}$. The eigenstates $|\psi_j\rangle$ of U are defined by

$$U \, |\psi_j\rangle = \mathrm{e}^{\mathrm{i}\varepsilon_j} \, |\psi_j\rangle \ , \qquad (5)$$

where ε_j are the quasi-energies having mean spacing $2\pi/N$. The eigenstates can be classified as either regular or chaotic depending on the region on which they predominately concentrate. Due to tunneling they have contributions in all regions of phase space.

A time-evolved wave packet, initially localized in the chaotic sea, will tunnel into the regular island. To measure its weight in the regular island we will later use its projection onto *regular basis states* $|\chi_m^{\mathrm{reg}}\rangle$, which are concentrated on quantized regular tori, see Fig. 2. These tori fulfill the WKB quantization rule

$$\oint p \, \mathrm{d}q = \left(m + \frac{1}{2}\right) h_{\mathrm{eff}} \ , \qquad (6)$$

with quantum number $m = 0, 1, ..., m_{\max} - 1$. The number of regular basis states in the island of area A_{reg} is given by

$$m_{\max} = \left\lfloor \frac{A_{\mathrm{reg}}}{h_{\mathrm{eff}}} + \frac{1}{2} \right\rfloor \ , \qquad (7)$$

where $\lfloor \cdot \rfloor$ denotes the floor function. We consider a designed map, Appendix A, for which $A_{\mathrm{reg}} \approx 0.21$. For $h_{\mathrm{eff}} = 1/20$ this leads to $m_{\max} = 4$ regular basis states. Generally, the construction of the regular basis states $|\chi_m^{\mathrm{reg}}\rangle$ can be done using semiclassical methods. For the designed map they are given analytically, Eq. (A8). The regular basis states $|\chi_m^{\mathrm{reg}}\rangle$ form an orthonormal basis within the regular island, they have no chaotic admixture, in contrast to the regular eigenstates of the quantum map.

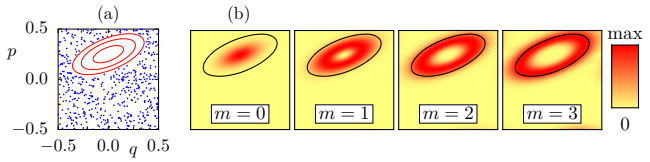

FIG. 2. (Color online) (a) Classical phase space of the designed map with chaotic dynamics (blue dots) and regular tori (red lines). (b) Husimi representation of all regular basis states $m = 0, 1, 2, 3$ for $h_{\mathrm{eff}} = 1/20$ (b). The border of the island is indicated by a solid line.

B. Wave packet dynamics

We consider the behavior of wave packets $|\varphi_t\rangle$, which are initially localized in the chaotic sea. Their weight on the mth regular torus is measured by the overlap with the mth regular basis state $|\chi_m^{\mathrm{reg}}\rangle$

$$p^{\mathrm{reg}}_{m,\theta_q,|\varphi_0\rangle}(t) = \left|\langle \chi_m^{\mathrm{reg}} \, | \, \varphi_t \rangle\right|^2 \ . \qquad (8)$$

This overlap depends on the initial wave packet $|\varphi_0\rangle$ and the chosen Bloch phase θ_q, which arises from the periodic boundary conditions in q-direction. Fig. 3 shows the probability $p^{\mathrm{reg}}_{m,\theta_q,|\varphi_0\rangle}(t)$ for $m = 0$ and different θ_q. We observe Rabi-like oscillations with various amplitudes and frequencies. They originate from the tunneling coupling of the regular basis state $|\chi_0^{\mathrm{reg}}\rangle$ with the spectrally closest chaotic state for each θ_q. These are superimposed by small oscillations caused by couplings to other chaotic states. In Fig. 3(b) we show $p^{\mathrm{reg}}_{m,\theta_q,|\varphi_0\rangle}(t)$ on a double logarithmic scale.

To investigate the universal behavior of the time evolution of wave packets flooding the regular island, we first introduce the *regular weight* p_m^{reg}

$$p_m^{\mathrm{reg}}(t) = \left\langle p^{\mathrm{reg}}_{m,\theta_q,|\varphi_0\rangle}(t) \right\rangle_{\theta_q,|\varphi_0\rangle} \ , \qquad (9)$$

which is the average over different Bloch phases θ_q and different initial wave packets $|\varphi_0\rangle$. In Fig. 3(b) the regular weight $p_0^{\mathrm{reg}}(t)$ shows a linear increase at small times and a saturation plateau at large times.

C. Flooding weight

To quantify the flooding in systems with a mixed phase space it is helpful to divide the Hilbert space into the regular basis states $|\chi_m^{\mathrm{reg}}\rangle$ and their complement containing

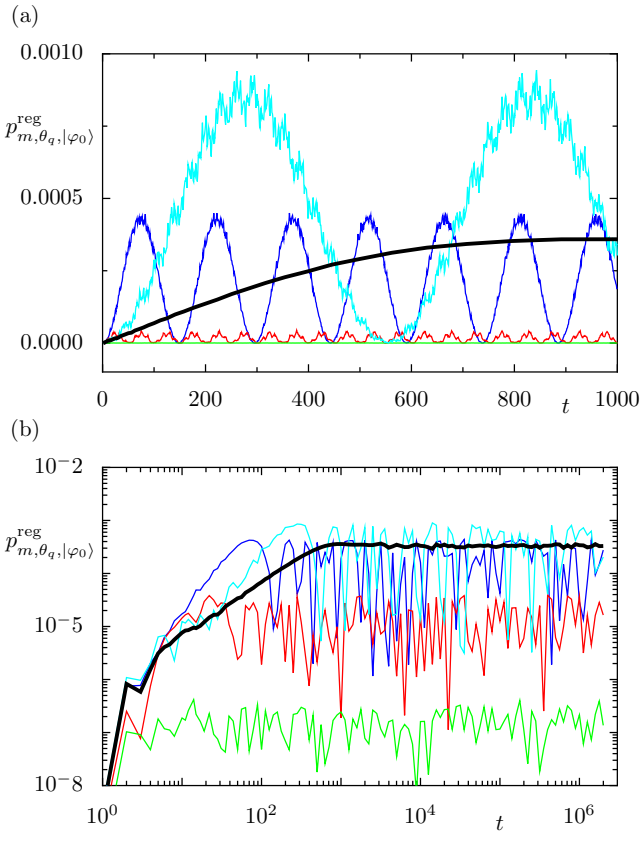

FIG. 3. (Color online) (a) The weight $p^{\rm reg}_{m,\theta_q,|\varphi_0\rangle}$ according to Eq. (8) on the regular torus $m = 0$ of the designed map with the initial state $|\varphi_0\rangle$ being a momentum eigenstate with $p \approx -0.25$ and under variation of the Bloch phase θ_q $(0.2, 0.3, 0.55, 0.75,$ blue, red, green, cyan) for $h_{\rm eff} = 1/20$. The black line shows the regular weight $p^{\rm reg}_m$ according to Eq. (9) averaged over 20000 pairs $\theta_q, |\varphi_0\rangle$. Here $\theta_q \in [0, 1)$ is chosen equidistantly and $|\varphi_0\rangle$ is a momentum eigenstate with $p \in [-0.45, -0.05]$ chosen randomly. (b) Double-logarithmic representation of the same data.

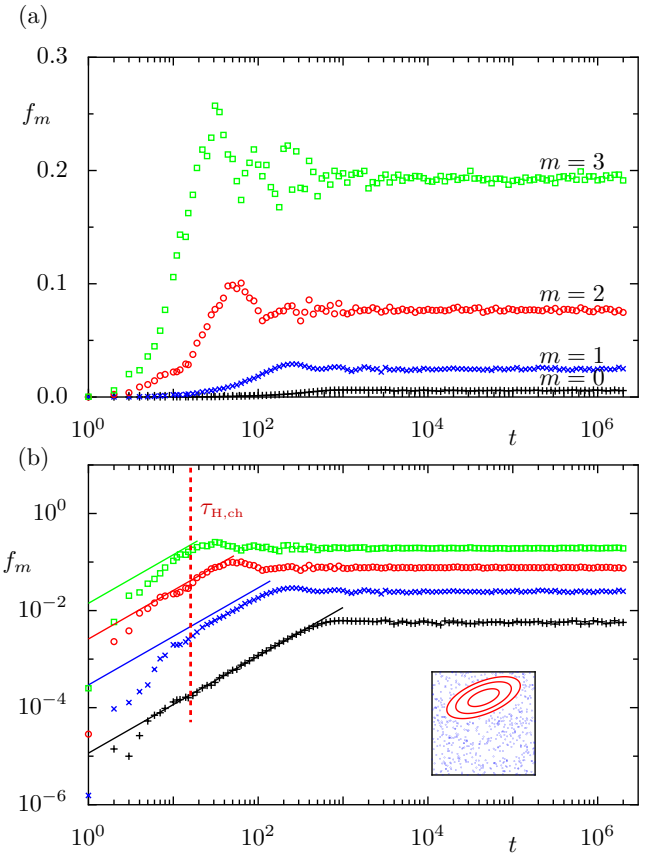

FIG. 4. (Color online) (a) Flooding weights for a wave packet started in the chaotic sea of the designed map with $h_{\rm eff} = 1/20$ for all regular basis states $m = 0, 1, 2, 3$. (b) Double-logarithmic representation of the same data together with the predictions of Eq. (20) (solid lines). The Heisenberg time $\tau_{\rm H,ch}$ is indicated by a dashed line. Inset: Phase space for $M = 1$.

the chaotic basis states $|\chi^{\rm ch}\rangle$. This separation allows for defining the *flooding weight* $f_m(t)$ which will turn out to show universal behavior,

$$f_m(t) = \frac{p^{\rm reg}_m(t)}{\frac{p^{\rm ch}(t)+p^{\rm reg}_m(t)}{N_{\rm ch}+1}} \ . \tag{10}$$

It is the ratio of the regular weight $p^{\rm reg}_m$ on the mth torus to the average weight in the subspace given by the chaotic basis states and the mth regular basis state. Here $p^{\rm ch}(t)$ is the weight in the chaotic subspace following from normalization

$$p^{\rm ch} + \sum_{m=0}^{m_{\rm max}-1} p^{\rm reg}_m = 1 \ . \tag{11}$$

and $N_{\rm ch}$ is the number of chaotic basis states, $N_{\rm ch} = N - m_{\rm max}$. The flooding weight $f_m(t)$, Eq. (10), has two advantages compared to the regular weight $p^{\rm reg}_m(t)$, Eq. (9): (i) The flooding weight $f_m(t)$ reaches $f_m = 1$ if the wave packet is uniformly spread over the chaotic sea and the mth regular torus. This is independent of the number of chaotic basis states. (ii) The flooding weight $f_m(t)$ does not depend on the flooding of other regular basis states unlike the regular weights $p^{\rm reg}_m(t)$, which has particular relevance if many tori are flooded, see Fig. 11 in Appendix B.

Fig. 4(a) shows the flooding weights $f_m(t)$ for different regular basis states. Fig. 4(b) shows a double-logarithmic representation of the same data and we observe a linear increase followed by a saturation of the flooding weights. For regular tori closer to the center of the island the asymptotic flooding weight is lower. The regime of linear increase and the saturation regime will be discussed in Secs. III and IV respectively. The transition regime shows in Fig. 4(a) remnants of Rabi-like oscillations as for $p^{\rm reg}_{m,\theta_q,|\varphi_0\rangle}$ in Fig. 3(a), which will be discussed in Sec. IV F.

D. Many unit cells in phase space

The amount of flooding of regular tori depends both on the tunneling rate and the size of the chaotic sea. A periodic extension of the designed map to M unit cells in q-direction, see inset of Fig. 5(b), increases the size of the chaotic sea. It thus increases the chaotic density of states and thereby the Heisenberg time $\tau_{\rm H,ch}$, while the tunneling rates remain unchanged for fixed $h_{\rm eff}$. Thus less and less regular eigenstates per unit cell exist according to Eq. (1) and we expect stronger temporal flooding [19, 20] with flooding weights reaching $f_m \approx 1$.

The generalization of the designed map to M unit cells in q-direction (Appendix A) leads to the following changes: (i) $h_{\rm eff} = M/N$, where M and N have no common divisor to avoid periodicities. (ii) We now use regular basis states $\chi^{\rm reg}_{m,j}$, which localize on the mth regular torus of the regular island of the jth unit cell. (iii) The regular weight is defined by summation over all M regular basis states with the same quantum number m

$$p^{\rm reg}_m(t) = \left\langle \sum_{j=0}^{M-1} \left| \langle \chi^{\rm reg}_{m,j} \,|\, \varphi_t \rangle \right|^2 \right\rangle_{\theta_q, |\varphi_0\rangle} \quad . \tag{12}$$

(iv) The flooding weight $f_m(t)$ is now defined by

$$f_m(t) = \frac{\frac{p^{\rm reg}_m(t)}{M}}{\frac{p^{\rm ch}(t) + p^{\rm reg}_m(t)}{N_{\rm ch}+M}} \quad , \tag{13}$$

which is the ratio of the average weight in the subspace of the M regular basis states on the mth regular torus to the average weight in the subspace given by the chaotic basis states and the M regular basis states with quantum number m. Here $p^{\rm ch}(t)$ is still given by Eq. (11) and $N_{\rm ch}$ is the number of chaotic basis states

$$N_{\rm ch} = N - M m_{\rm max} \quad . \tag{14}$$

The definition of the flooding weight $f_m(t)$ is such that it reaches $f_m = 1$, if the wave packet is uniformly spread over the chaotic sea and the mth regular torus in all M unit cells. (v) The periodic extension leads to transporting regular islands, e.g. the mth torus in the jth unit cell is mapped to the $(j+1)$th unit cell. The case of non-transporting islands is discussed in Ref. [34].

Fig. 5 shows the flooding weights for the designed map with $M = 144$. The qualitative behavior is similar to Fig. 4 with $M = 1$, but due to the large chaotic sea one reaches flooding weights closer to one.

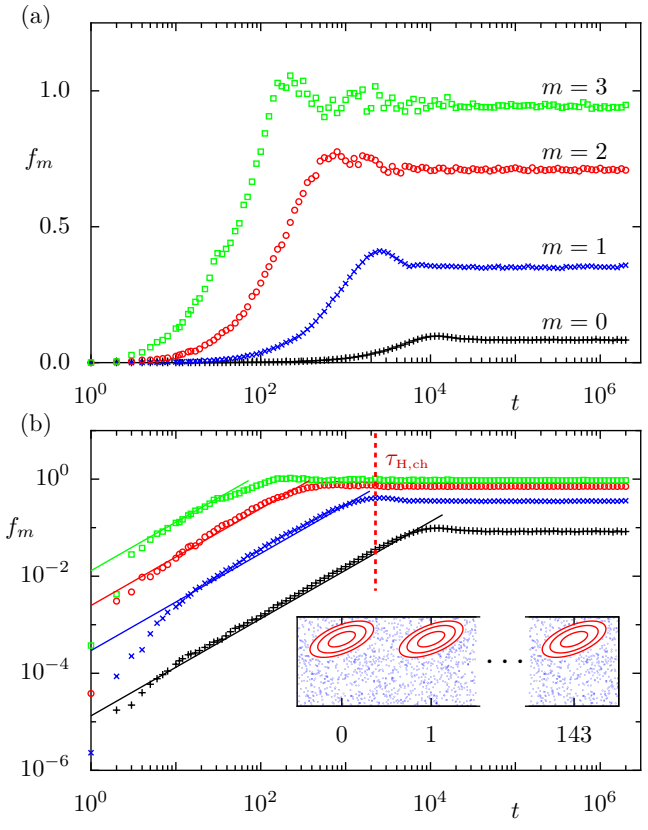

FIG. 5. (Color online) (a) Flooding weights for a wave packet started in the chaotic sea of the designed map with $h_{\rm eff} = 144/2825 \approx 1/20$ and $M = 144$ for all regular basis states $m = 0, 1, 2, 3$. (b) Double-logarithmic representation of the same data together with the predictions of Eq. (20) (solid lines). The Heisenberg time $\tau_{\rm H,ch}$ is indicated by a dashed line.

III. LINEAR REGIME

The linear increase of the flooding weights $f_m(t)$ observed in Figs. 4(b) and 5(b) is a consequence of the linear increase of the regular weights $p^{\rm reg}_m(t)$ at small times due to dynamical tunneling

$$p^{\rm reg}_m(t) = \gamma^{\rm ch\to reg}_m \, t \quad , \tag{15}$$

with the chaotic-to-regular tunneling rate $\gamma^{\rm ch\to reg}_m$. From Eq. (13) with $p^{\rm reg}_m \ll p^{\rm ch}(t) \approx 1$ follows for the flooding weight

$$f_m(t) \approx \frac{N_{\rm ch} + M}{M} \gamma^{\rm ch\to reg}_m \, t \quad . \tag{16}$$

We now express the chaotic-to-regular tunneling rate $\gamma^{\rm ch\to reg}_m$ by the regular-to-chaotic tunneling rate $\gamma^{\rm reg\to ch}_m = \gamma_m$. Both rates are related to the same tunneling coupling matrix element $v^{\rm reg,ch}_m = \langle \chi^{\rm reg}_m | \, U \, | \chi^{\rm ch} \rangle$ by Fermi's golden rule in dimensionless form (see Appendix A in [35])

$$\gamma^{\rm ch\to reg}_m = 2\pi \left\langle \left| v^{\rm reg,ch}_m \right|^2 \right\rangle \rho^{\rm reg}_m \tag{17}$$

$$\gamma_m = \gamma^{\rm reg\to ch}_m = 2\pi \left\langle \left| v^{\rm reg,ch}_m \right|^2 \right\rangle \rho^{\rm ch} \quad . \tag{18}$$

Here $\rho^{\rm ch} = N_{\rm ch}/(2\pi)$ is the density of chaotic basis states and $\rho_m^{\rm reg} = M/(2\pi)$ is the density of regular basis states corresponding to the mth torus. This leads to

$$\gamma_m^{\rm ch\to reg} = \gamma_m \frac{\rho_m^{\rm reg}}{\rho^{\rm ch}} = \gamma_m \frac{M}{N_{\rm ch}} \tag{19}$$

and allows for rewriting Eq. (16) as

$$f_m(t) \approx \frac{N_{\rm ch}+M}{N_{\rm ch}} \gamma_m \, t \quad . \tag{20}$$

For $M \ll N_{\rm ch}$ this simplifies to $f_m(t) \approx \gamma_m t$. In the following we use the numerically obtained tunneling rates γ_m, see [35, 36]. For the parameters of Fig. 4 we find $\gamma_0 = 1.16 \cdot 10^{-5}, \gamma_1 = 2.94 \cdot 10^{-4}, \gamma_2 = 2.60 \cdot 10^{-3}, \gamma_3 = 1.41 \cdot 10^{-2}$. For the parameters of Fig. 5, where $h_{\rm eff}$ is changed by 2% one finds that the tunneling rates γ_m change by less than 15%. Figures 4(b) and 5(b) show that this linear behavior, Eq. (20), is valid almost up to the saturation regime.

Naively, one would expect that the saturation happens latest at the Heisenberg time, which in dimensionless form is given by $\tau_{\rm H,ch} = N_{\rm ch}$. Fig. 5(b) and in particular Fig. 4(b) show that this is not true and that the saturation regime may be reached at much larger times. This will be explained in Sec. IV E.

IV. SATURATION REGIME

In this section we study the saturation regime of the flooding weights. By introducing an appropriate scaling parameter we find universal properties for the asymptotic behavior of the flooding weights.

A. Universal scaling of the asymptotic flooding weight

The flooding weights saturate on plateaus of different heights shown in Fig. 5. We define the *asymptotic flooding weight*

$$f_m^\infty = \langle f_m(t) \rangle_t \quad , \tag{21}$$

where $\langle \cdot \rangle_t$ indicates a temporal average. Numerically one uses a time interval, which starts at times larger than the beginning of each plateau.

As scaling parameter for the asymptotic flooding weights we define an effective coupling $v_{\rm eff}$ between regular and chaotic basis states

$$v_{{\rm eff},m} = \frac{\sqrt{\langle |v_m^{\rm reg,ch}|^2 \rangle}}{\Delta_{\rm eff}} \quad . \tag{22}$$

It is obtained by rescaling the averaged tunnel coupling matrix elements $v_m^{\rm reg,ch}$ with the mean level spacing

$$\Delta_{\rm eff} = \frac{2\pi}{N_{\rm ch}+M} \tag{23}$$

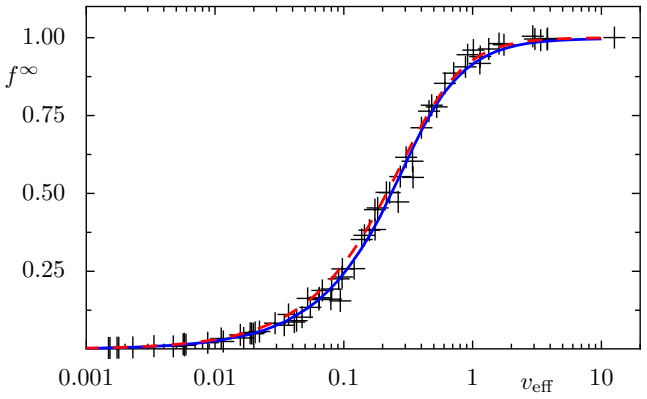

FIG. 6. (Color online) Asymptotic flooding weights f^∞ vs. effective coupling $v_{\rm eff}$ of the designed map for various parameters $h_{\rm eff} = 1/10, 1/20, 1/30, 1/40$, $M = 1, 13, 144, 1597, 17711$, and $m = 1, \ldots, 8$ (black crosses), random matrix prediction (blue solid line) and Eq. (42) (red dashed line).

in a subsystem of $N_{\rm ch}$ chaotic and M regular basis states on the mth regular torus. This effective coupling $v_{\rm eff}$ is almost identical to the square root of the transition parameter $\Lambda = v^2/\Delta^2$ of coupled random matrix models for mixed systems [6] with v^2 the variance of the perturbation and Δ the mean level spacing. However, here the effective mean level spacing $\Delta_{\rm eff}$, Eq. (23), of the subsystem is more appropriate than the mean level spacing $\Delta = 2\pi/N$. Note, that the definition of $\Delta_{\rm eff}$ in Eq. (23) is also different from the one in Ref. [20, Sec. 4] where $\Delta_{\rm ch} = 2\pi/N_{\rm ch}$ is used as the effective mean level spacing. For the parameters used there it is irrelevant as $M \ll N_{\rm ch}$, while for $M \approx N_{\rm ch}$ we find that it is necessary to use Eq. (23).

Often it is convenient to express the effective coupling $v_{\rm eff}$ in terms of the numerically accessible tunneling rates γ_m instead of the coupling matrix element $v_m^{\rm reg,ch}$. Using Fermi's golden rule, Eq. (18), leads to

$$v_{{\rm eff},m} = \frac{N_{\rm ch}+M}{2\pi\sqrt{N_{\rm ch}}} \sqrt{\gamma_m} \quad . \tag{24}$$

Fig. 6 shows that there is a universal dependence of the asymptotic flooding weights f^∞ as a function of the effective coupling $v_{\rm eff}$ for the designed map. This is observed for various parameter values for $h_{\rm eff}$, M, $m_{\rm max}$, and m over several orders of magnitude in $v_{\rm eff}$. Note that the transition is rather broad in $v_{\rm eff}$.

B. Asymptotic flooding weight in terms of eigenstates

For various applications it is convenient to express the asymptotic flooding weight in terms of properties of the eigenstates, instead of the time evolution of wave packets. This will include the numerical and analytical study of random matrix models and the numerical study of the mushroom billiard.

For simplicity let us start with the case $M = 1$. Furthermore we restrict ourselves to one individual regular torus m for the remainder of this section, which is justified by the universal behavior of f^∞ demonstrated in Fig. 6. Then the Hilbert space of size N is spanned by an orthogonal basis given by one regular basis state $|\chi^{\rm reg}\rangle$ and $N_{\rm ch} = N - 1$ chaotic basis states $|\chi^{\rm ch}\rangle$.

The initial wave packet $|\varphi_0\rangle$ at $t = 0$ is assumed to be a random superposition of chaotic basis states $|\chi_r^{\rm ch}\rangle$

$$|\varphi_0\rangle = \sum_{r=1}^{N_{\rm ch}} a_r \mathrm{e}^{\mathrm{i}\xi_r} |\chi_r^{\rm ch}\rangle \quad , \tag{25}$$

where $\xi_r \in [0, 2\pi)$ are identical independently distributed random variables for $r = 1, \ldots, N_{\rm ch}$. The random real amplitudes a_r only have to fulfill the normalization condition $\sum_{r=1}^{N_{\rm ch}} a_r^2 = 1$ such that

$$\langle a_r^2 \rangle_{|\varphi_0\rangle} = 1/N_{\rm ch}. \tag{26}$$

The expansion coefficients c_k of the initial wave packet $|\varphi_0\rangle$ in the basis of eigenstates $|\psi_k\rangle$ of U are

$$c_k = \langle \psi_k \,|\, \varphi_0 \rangle = \sum_{r=1}^{N_{\rm ch}} a_r \mathrm{e}^{\mathrm{i}\xi_r} \left\langle \psi_k \,\middle|\, \chi_r^{\rm ch} \right\rangle \quad , \tag{27}$$

for $k = 1, \ldots, N$. The average over the initial wave packet $|\varphi_0\rangle$ leads to

$$\left\langle |c_k|^2 \right\rangle_{|\varphi_0\rangle} = \left\langle \sum_{r,s=1}^{N_{\rm ch}} a_r a_s \mathrm{e}^{\mathrm{i}(\xi_r - \xi_s)} \left\langle \psi_k \,\middle|\, \chi_r^{\rm ch} \right\rangle \left\langle \chi_s^{\rm ch} \,\middle|\, \psi_k \right\rangle \right\rangle_{|\varphi_0\rangle} \tag{28}$$

$$= \frac{1}{N_{\rm ch}} \sum_{r=1}^{N_{\rm ch}} \left| \left\langle \chi_r^{\rm ch} \,\middle|\, \psi_k \right\rangle \right|^2 \tag{29}$$

$$= \frac{1}{N_{\rm ch}} \left(1 - |\langle \chi^{\rm reg} \,|\, \psi_k \rangle|^2 \right) \quad , \tag{30}$$

where in the first step the off-diagonal terms of the double sum vanish due to the random phases ξ_r and for the diagonal term we used Eq. (26). In the second step the completeness and orthogonality of the regular and chaotic basis states was taken into account.

To compute the asymptotic flooding weight f^∞ we consider an ensemble of quantum maps with associated eigenstates $|\psi_k\rangle$. Within this ensemble the regular states and their average coupling to the chaotic states are fixed, while the chaotic states are strongly varied. For an individual quantum map the overlap of the time-evolved wave packet $|\varphi_t\rangle = \sum_{k=1}^N c_k \mathrm{e}^{\mathrm{i}\varepsilon_k t} |\psi_k\rangle$ with the regular basis states is according to Eq. (8) given by

$$p^{\rm reg}_{|\varphi_0\rangle}(t) = |\langle \chi^{\rm reg} \,|\, \varphi_t \rangle|^2 \tag{31}$$

$$= \sum_{k,l=1}^{N} c_k c_l^* \mathrm{e}^{\mathrm{i}(\varepsilon_k - \varepsilon_l)t} \langle \chi^{\rm reg} \,|\, \psi_k \rangle \langle \psi_l \,|\, \chi^{\rm reg} \rangle \tag{32}$$

$$= \sum_{k=1}^{N} |c_k|^2 \, |\langle \chi^{\rm reg} \,|\, \psi_k \rangle|^2 + p_{\rm fl}(t) \quad , \tag{33}$$

where

$$p_{\rm fl}(t) = \sum_{k \neq l} c_k c_l^* \mathrm{e}^{\mathrm{i}(\varepsilon_k - \varepsilon_l)t} \langle \chi^{\rm reg} \,|\, \psi_k \rangle \langle \psi_l \,|\, \chi^{\rm reg} \rangle \quad . \tag{34}$$

As in Eq. (9) we now perform an average over different initial wave packets $|\varphi_0\rangle$ and perform an ensemble average (indicated by $\langle\cdot\rangle_e$), giving the regular weight

$$p^{\rm reg}(t) = \left\langle p^{\rm reg}_{|\varphi_0\rangle}(t) \right\rangle_{e,|\varphi_0\rangle} \quad . \tag{35}$$

Following Eq. (10) and using that $p^{\rm reg}(t) + p^{\rm ch}(t) = 1$ we obtain the flooding weight

$$f(t) = (N_{\rm ch} + 1) p^{\rm reg}(t) \quad . \tag{36}$$

For the asymptotic flooding weight we perform a time average according to Eq. (21), $f^\infty = \langle f(t) \rangle_t$, and with $\langle p_{\rm fl}(t) \rangle_t = 0$ we obtain

$$f^\infty = (N_{\rm ch} + 1) \left\langle \sum_{k=1}^{N} |c_k|^2 \, |\langle \chi^{\rm reg} \,|\, \psi_k \rangle|^2 \right\rangle_{e,|\varphi_0\rangle} \quad . \tag{37}$$

Using Eq. (30) we finally obtain

$$f^\infty = \frac{N_{\rm ch} + 1}{N_{\rm ch}} \left(1 - \left\langle \sum_{k=1}^{N} |\langle \chi^{\rm reg} \,|\, \psi_k \rangle|^4 \right\rangle_e \right) \quad . \tag{38}$$

This gives the dependence of the asymptotic flooding weight f^∞ on the overlap of the eigenstates with the regular basis states. The extreme values of f^∞ are zero and one: If an eigenstate of the system is identical to a regular basis state it is not flooded at all and $f^\infty = 0$. In contrast, for a completely flooded state, i.e. $|\chi^{\rm reg}\rangle$ has the same overlap $1/N$ with all eigenstates $|\psi_j\rangle$, we get $f^\infty = 1$.

For the more general case with more than one regular basis state on the same regular torus in different unit cells ($M \neq 1$) we obtain with this approach the asymptotic flooding weight

$$f^\infty = \frac{N_{\rm ch} + M}{N_{\rm ch}} \left(1 - \langle p \rangle_e \right) \tag{39}$$

$$p = \sum_{k=1}^{N} \frac{1}{M} \left(\sum_{j=1}^{M} \left| \left\langle \chi_j^{\rm reg} \,\middle|\, \psi_k \right\rangle \right|^2 \right)^2 \quad . \tag{40}$$

This concludes the derivation of an expression of the asymptotic flooding weight in terms of properties of the eigenstates, which is complementary to its definition in terms of the time evolution of wave packets, Eq. (21).

C. Random matrix modeling

Random matrix modeling has been successfully used to describe level statistics in the context of chaos assisted

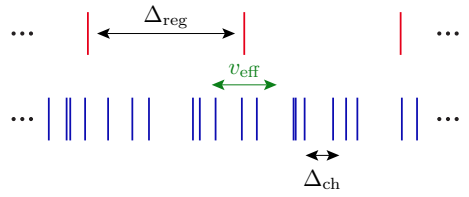

FIG. 7. (Color online) The regular spectrum of the mth torus of a transporting island is equidistant with spacing $\Delta_{\rm reg}$ and the chaotic spectrum is modeled by the circular orthogonal ensemble with mean spacing $\Delta_{\rm ch}$. The typical regular to chaotic coupling is $v_{\rm eff}$.

tunneling, see e.g. [6, 20, 37–39]. To explain the behavior of the asymptotic flooding weights we use the model proposed in Ref. [20] given by the time dependent Hamiltonian

$$H = \begin{pmatrix} H_{\rm reg} & V \\ V^T & H_{\rm ch} \end{pmatrix} \quad . \tag{41}$$

Here $H_{\rm reg}$ is a diagonal matrix with entries representing the eigenenergies of a purely regular system, where the matrix size is given by $Mm_{\rm max}$. In the following we restrict ourselves to the study of one individual regular torus, such that the matrix size of $H_{\rm reg}$ is M. In the case of transporting regular islands the energies of these M regular basis states are equidistant [40], see Fig. 7. In this matrix model we choose the energy spacings such that the mean spacing $\Delta_{\rm eff} = 1$ and the regular basis states are spread over an energy interval of length N. This is in contrast to the Poissonian distribution, which generically occurs if one considers many quantized regular tori. The case of non-transporting islands is discussed in Ref. [34].

For $H_{\rm ch}$ we use a diagonal matrix of size $N_{\rm ch}$, with entries representing the eigenvalues of a purely chaotic system. Instead of using eigenvalues of a matrix from the Gaussian orthogonal ensemble, as commonly used, we take the eigenvalues of a matrix from the circular orthogonal ensemble [41] scaled to the energy interval of length N such that $\Delta_{\rm ch} = N/N_{\rm ch}$. This ensures that we can use all eigenstates, as the mean level spacing is constant in contrast to the semi-circle law of the Gaussian orthogonal ensemble. Boundary effects can be neglected for sufficiently large matrix size N. The coupling matrix V consists of Gaussian random variables with mean zero and variance $(v_{\rm eff}\Delta_{\rm eff})^2$ according to Eq. (23), which for the chosen energy scaling gives the variance $v_{\rm eff}^2$. Numerically we used for the ratio of the submatrix sizes $N_{\rm ch}/M = 1$ and found convergence at matrix size $N = 400$ even for the largest effective couplings $v_{\rm eff}$. For ratios $N_{\rm ch}/M > 1$ convergence of f^∞ is obtained for larger N only, e.g. for $N_{\rm ch}/M = 5$ a matrix size $N = 10000$ is needed.

Fig. 6 shows the predictions of the random matrix model for the asymptotic flooding weights, Eq. (39). They are in good agreement with the asymptotic flooding weights obtained by time evolution of wave packets of the designed map.

D. 2×2 matrix model

It turns out that a 2×2 matrix model leads to the asymptotic flooding weight

$$f^\infty_{2\times 2}(v_{\rm eff}) = 2v_{\rm eff} \arctan \frac{1}{2v_{\rm eff}} \tag{42}$$

which very closely follows the numerical flooding weights of the designed map and the prediction of the random matrix model, see Fig. 6. Equation (42) is the answer to the question of the universeality [42]. It follows from a reduction of the random matrix model, Eq. (41), to a 2×2 matrix model

$$H = \begin{pmatrix} \kappa & v \\ v & -\kappa \end{pmatrix} \quad , \tag{43}$$

where 2κ is the unperturbed spacing and v the coupling matrix element of a chaotic state $|\chi^{\rm ch}\rangle$ and the closest regular state $|\chi^{\rm reg}\rangle$. Their spacing 2κ is uniformly distributed in the interval $[0, 1]$ if the number of regular and chaotic states is equal and the mean level spacing is one. For the 2×2 matrix model we therefore chose κ to be a uniformly distributed random variable in the interval $[0, 1/2]$. Choosing a constant $v = v_{\rm eff}$ gives Eq. (42), see below. We observe that it agrees better with the numerical data than the result obtained for a Gaussian random variable v.

The asymptotic flooding weights for this model can be obtained using Eq. (38). The overlaps $|\langle \chi^{\rm reg} \,|\, \psi_\pm \rangle|^2$ of the eigenstates $|\psi_\pm\rangle$ of H for the 2×2 matrix are given by

$$|\langle \chi^{\rm reg} \,|\, \psi_\pm \rangle|^2 = \frac{v^2}{2} \left(\kappa^2 + v^2 \pm \kappa \sqrt{\kappa^2 + v^2} \right)^{-1} \quad . \tag{44}$$

After some algebra Eq. (38) with $N_{\rm ch} = 1$ leads for the asymptotic flooding weight to

$$f^\infty_{2\times 2} = 2 \left(1 - \left\langle \frac{\kappa^2 + \frac{v^2}{2}}{\kappa^2 + v^2} \right\rangle_e \right) \quad , \tag{45}$$

which after the ensemble average $\langle \cdot \rangle_e = 2 \int_0^{1/2} {\rm d}\kappa \, \cdot$ leads to Eq. (42). The limits for small and strong effective coupling are

$$f^\infty_{2\times 2} \overset{v_{\rm eff} \ll 1}{=} \pi v_{\rm eff} \tag{46}$$

$$f^\infty_{2\times 2} \overset{v_{\rm eff} \gg 1}{=} 1 - 1/(12 v_{\rm eff}^2) \quad . \tag{47}$$

The agreement of Eq. (42) with the numerical calculations for the designed map obtained by time evolution, see Fig. 6, is surprisingly good even for strong coupling, where couplings to many chaotic states are relevant, while they are not considered in the above 2×2 matrix model. This is reminiscent to the success of the Wigner surmise for level spacing statistics which is also based on a 2×2 matrix model.

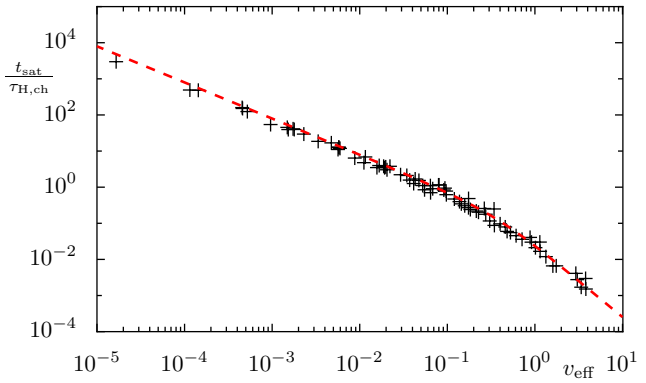

FIG. 8. (Color online) Ratio of saturation time $t_{\rm sat}$ to Heisenberg time $\tau_{\rm H,ch}$ vs. effective coupling $v_{\rm eff}$ of the designed map for various parameters $h_{\rm eff} = 1/10, 1/20, 1/30, 1/40$, $M = 1, 13, 144, 1597, 17711$, and $m = 1, \ldots, 8$ (black crosses) and Eq. (49) (red dashed line).

E. Saturation time

We now discuss the time scale $t_{\rm sat}$ for reaching the saturation plateau. For the mth regular torus we define $t_{{\rm sat},m}$ by the time at which the initial linear behavior, Eq. (20), intersects the asymptotic flooding weight f_m^∞, leading to

$$t_{{\rm sat},m} = \frac{N_{\rm ch} f_m^\infty}{(N_{\rm ch}+M)\gamma_m} \quad . \tag{48}$$

By expressing γ_m in terms of $v_{\rm eff}$, Eq. (24), and dividing by the Heisenberg time $\tau_{\rm H,ch} = N_{\rm ch} + M$ we find the universal scaling

$$\frac{t_{\rm sat}}{\tau_{\rm H,ch}} = \frac{f^\infty(v_{\rm eff})}{4\pi^2 v_{\rm eff}^2} \approx \frac{f^\infty_{2\times 2}(v_{\rm eff})}{4\pi^2 v_{\rm eff}^2} = \frac{\arctan\frac{1}{2v_{\rm eff}}}{2\pi^2 v_{\rm eff}} \quad , \tag{49}$$

where in the last step Eq. (42) from the 2×2 model is used.

Numerically, the saturation times are determined by the intersection time of a fitted linear increase with the saturation plateau. Fig. 8 shows the numerical saturation times for the designed map in comparison to Eq. (49). Very good agreement is found. At first, it might be surprising, that the saturation time can be much larger than the Heisenberg time. However, these large time scales arise from small splittings of weakly coupled regular and chaotic states, which are much smaller than the mean level spacing.

F. Transition regime

At the saturation time one has a transition from the linear regime to the saturation regime. In Figs. 4(a) and 5(a) one observes an overshooting of the flooding weights beyond their asymptotic value. It can be understood by Rabi-like oscillations that occur in the 2×2 model, Eq. (43). For fixed coupling v one obtains damped but long-lasting oscillations. For Gaussian averaged couplings v the resulting curve resembles the numerically obtained flooding weights, e.g. as in Fig. 5(a) for $m = 1$ [34].

The extreme case of complete flooding is studied in Appendix B. In this case, no overshooting of the flooding weights is observed, see Fig. 11. The behavior around the transition can be very well described by a master-equation approach. In particular, one obtains an approximate analytical expression for the flooding weights,

$$f_m(t) = 1 - \exp\left(-\frac{N_{\rm ch}+M}{N_{\rm ch}}\gamma_m^{\rm reg\to ch} t\right) \tag{50}$$

for all m, see Fig. 11.

V. APPLICATIONS

A. Standard map

The Chirikov standard map [43]

$$q_{n+1} = q_n + p_n \tag{51}$$

$$p_{n+1} = p_n + \frac{K}{2\pi}\sin\left(2\pi[q_n+p_n]\right) \tag{52}$$

is considered on the torus $[-1/2, 1/2]\times[0,1]$, i.e. with one unit cell $M = 1$. It arises from the kicked Hamiltonian

$$H(q,p,t) = \frac{p^2}{2} + \frac{K}{(2\pi)^2}\cos(2\pi q)\sum_{n\in\mathbb{Z}}\delta(t-n) \quad , \tag{53}$$

with kicking strength K. The quantum time evolution is given by Eq. (4).

In Fig. 9 the flooding weights are shown for different regular tori. The qualitative behavior is the same as for the designed map with an initial linear increase followed by a saturation plateau. For the theoretical prediction,

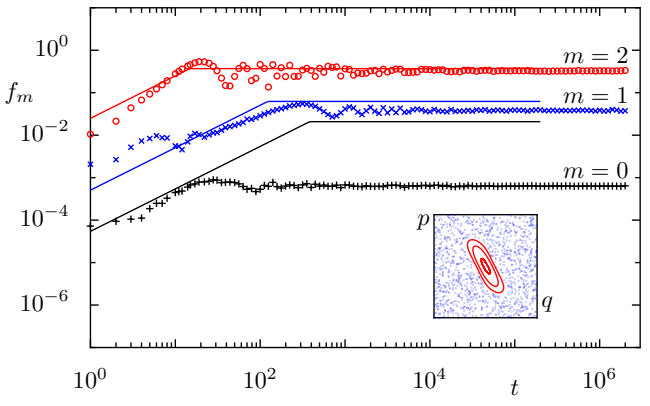

FIG. 9. (Color online) Flooding weights $f_m(t)$ of the standard map for $K = 2.9$, $N = 29$, and $M = 1$, for the regular tori $m = 0, 1, 2$ (symbols). They are compared to the prediction of Eqs. (20) and (42) (solid lines).

Eqs. (20) and (42), we use the numerically obtained tunneling rates [35, 36] Quantitatively we observe the largest deviation for $m = 0$. We explain this discrepancy by the less effective Bloch phase averaging, which only leads to few avoided crossings for the standard map. This might be improved by a modified standard map [26] which allows for better averaging.

As an aside we mention that the detailed behavior of the flooding weights for $m = 1$ can be understood by the use of 2×2 matrix models [34].

B. Mushroom billiard

The phenomenon of flooding also appears in time-independent systems with a mixed phase space such as two-dimensional billiards. As an example we investigate the mushroom billiard, see inset in Fig. 10. It is proven to have a sharply divided phase space [44]. Quantum mechanically a particle of mass μ in the billiard can be described by the time-independent Schrödinger equation, $\Delta\psi_i = E_i\psi_i$, with units $\hbar = 2\mu = 1$. Numerically, the eigenfunctions ψ_i are computed using the improved method of particular solutions [45, 46]. The regular basis states are given by the eigenfunctions of the quarter circle billiard

$$\chi^{\mathrm{reg}}_{n,m}(\rho,\varphi) \propto \mathbf{J}_m(j_{mn}\rho)\sin(m\varphi) \quad . \tag{54}$$

in polar coordinates (ρ, φ), where $\mathbf{J}_m$ is the mth Bessel function and j_{mn} is its n-th root. For the determination of the asymptotic flooding weights f^∞ it is numerically inconvenient to use the time-evolution of wave packets. Instead we use the eigenfunctions ψ_i and determine the asymptotic flooding weight f^∞ applying Eq. (38) to a billiard, where $N_{\mathrm{ch}} \to \infty$,

$$f^\infty = \left(1 - \sum_{i=0}^{\infty} \left\langle \left| \langle \chi^{\mathrm{reg}}_{n,m} \,|\, \psi_i \rangle \right|^4 \right\rangle_e \right) \quad . \tag{55}$$

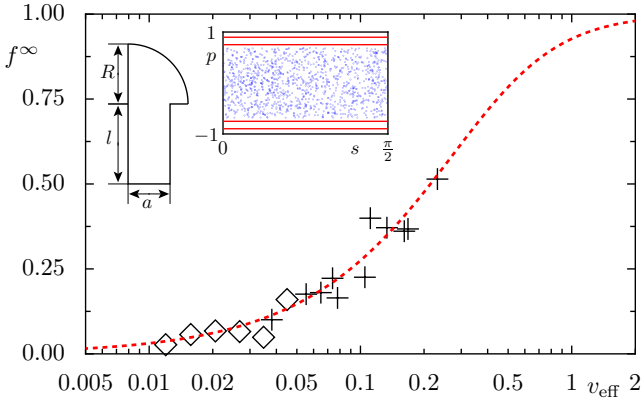

FIG. 10. (Color online) Asymptotic flooding weights f^∞ (symbols) for the mushroom billiard (inset) with $R = 1$, $a = 0.7$ vs. v_{eff} compared to the prediction Eq. (42) (red dashed line). As explained in the text, v_{eff} is either determined analytically (diamonds) or numerically (crosses).

Here the ensemble average $\langle\cdot\rangle_e$ is implemented as a variation of the stem length $l \in [1.4, 2.3]$ for 450 parameters with fixed $R = 1$ and $a = 0.7$. Fig. 10 demonstrates the same universal scaling of the asymptotic flooding weight f^∞ with the effective coupling v_{eff} for the mushroom billiard as observed for the quantum map in Fig. 6. Asymptotic flooding weights $f^\infty > 0.6$ could not be achieved as this would require much larger lengths of the stem, which are numerically hard to study. For Fig. 10 we have computed the effective coupling v_{eff} in two different ways: (i) For small couplings we use in Eq. (24) the analytical result for the tunneling rates (Eq. (8) in Ref. [47]). (ii) For larger couplings, where this analytical result is not accurate enough, we determine v_{eff} from Eq. (22) using the numerically determined averaged width of avoided crossings of the corresponding regular states under variation of the length of the stem [35, 47].

VI. SUMMARY AND OUTLOOK

The temporal flooding of regular tori by chaotic wave packets is analyzed in detail. The overlap of a wave packet started in the chaotic sea with a regular basis state concentrated on a quantizing torus can show Rabi-like oscillations with various amplitudes and frequencies. We average this overlap over different initial states and over an ensemble of quantum systems, which differ in the chaotic region only, e.g. by varying a Bloch phase. By a suitably defined normalization we introduce the flooding weight, which shows universal behavior.

Initially, it increases linearly depending on the regular-to-chaotic tunneling rate. Later it saturates and we find that the asymptotic flooding weight shows a universal scaling with a suitably defined effective coupling. This is found for a designed quantum map, the standard map, and the mushroom billiard. The universal scaling of the asymptotic flooding weight is reproduced by a random matrix model and well described by a simple function, Equation (42), that follows from a $2\times$ 2 matrix model. We also find that the saturation time, at which the initial linear increase turns into saturation, shows universal behavior that can be well described analytically.

Beyond the present study of wave packets started in the chaotic sea, one could study wave packets started on the regular island. They will partially tunnel to the chaotic sea. Their asymptotic weight in the chaotic sea, however, will depend sensitively on the initial wave packet. Universal behavior could be expected for the time evolution of the regular basis states. The initial linear increase in the chaotic region will be governed by the corresponding regular-to-chaotic tunneling rate. The scaling of the asymptotic weight in the chaotic sea needs

to be investigated. An experimental investigation of the consequences of flooding using a mushroom shaped microwave cavity will be published elsewhere [48].

ACKNOWLEDGMENTS

We thank Steffen Löck for code to determine regular basis states in the standard map and eigenfunctions of the mushroom billiard. We are grateful for discussions with Martin Körber, Ulrich Kuhl, and Hans-Jürgen Stöckmann. Furthermore, we acknowledge support by the Deutsche Forschungsgemeinschaft within the Forschergruppe 760 "Scattering Systems with Complex Dynamics.'

Appendix A: Designed map

In this appendix we give the explicit definition of the designed map and discuss some of its quantum properties.

For a kicked Hamiltonian, Eq. (2) a stroboscopic view after each kick gives

$$q_{n+1} = q_n + T'(p_n) \ , \tag{A1a}$$
$$p_{n+1} = p_n - V'(q_{n+1}) \ . \tag{A1b}$$

We consider the mapping on the torus $[-\frac{1}{2}, M-\frac{1}{2}] \times [-\frac{1}{2}, \frac{1}{2}]$. Thus the phase space extends over M unit cells in q-direction. The dynamics exclusively depends on the choice of the functions $T'(p_n)$ and $V'(q_{n+1})$.

A phase space with a large regular island can be designed [20, 29] with the functions

$$v(q) = -k(q)\left(\frac{k(q)}{2} + x(q)\right) - \frac{r x(q)^2}{2} \ , \tag{A2a}$$
$$t(p) = \begin{cases} -\frac{p}{2} + p^2 - \frac{5}{16} & (p \le 0) \\ \frac{3p}{2} - p^2 - \frac{5}{16} & (p > 0) \end{cases} \ , \tag{A2b}$$

where $r = 0.65$ and

$$k(q) = \left\lfloor q + \frac{1}{2} \right\rfloor \tag{A3a}$$
$$x(q) = q - k(q) = q - \left\lfloor q + \frac{1}{2} \right\rfloor \ , \tag{A3b}$$

where $\lfloor \cdot \rfloor$ denotes the floor function. To obtain smooth functions we define

$$T(p) = \int_{-\infty}^{\infty} \mathrm{d}z \, t(p+z) G_\epsilon(z), \tag{A4a}$$
$$V(q) = \int_{-\infty}^{\infty} \mathrm{d}z \, v(q+z) G_\epsilon(z). \tag{A4b}$$

where $G_\epsilon(z) = \exp(-z^2/2\epsilon^2)/\sqrt{2\pi\epsilon^2}$ is a Gaussian of width $\epsilon = 0.015$. The average value of $T'(p)$ defines the transport behavior in q-direction of the mapping. For the considered map the local average velocity in the lower part of phase space ($-1/2 < p < 0$) is -1, while in the upper part ($0 < p < 1/2$) it is $+1$. This leads to transport of the regular island to the right and in the chaotic sea the diffusive transport is biased to the left. The total phase-space velocity averages to zero.

Quantum mechanically the time evolution of a state is given by Eq. (4) in terms of the unitary operator Eq. (3). The eigenstates $|\psi_j\rangle$ of this operator are defined by Eq. (5). In order to fulfill the periodicity of the classical dynamics, the quantum states have to obey the quasi-periodicity conditions

$$\langle p+1|\psi\rangle = \mathrm{e}^{-2\pi\mathrm{i}\theta_p}\langle p|\psi\rangle \ . \tag{A5}$$
$$\langle q+M|\psi\rangle = \mathrm{e}^{2\pi\mathrm{i}\theta_q}\langle q|\psi\rangle \ , \tag{A6}$$

where θ_q and θ_p are Bloch phases. The effective Planck's constant can only be a rational number

$$h_{\mathrm{eff}} = \frac{M}{N} \ . \tag{A7}$$

We consider the case of coprime M and N, so that the quantum system is not effectively reduced to less than M cells.

The designed map allows for finding an analytic expression of the regular basis states using harmonic oscillator states that are squeezed in p-direction, rotated around the origin, and shifted to the center of the regular island in the jth unit cell, $q = j, p = 0.25$. Neglecting the periodic boundary conditions on the torus their position representation is given by [20]

$$\langle q \,|\, \chi^{\mathrm{reg}}_{m,j}\rangle = \sqrt{\frac{M}{2^m m! N}} \left(\frac{\mathfrak{Re}\ c}{\pi\hbar_{\mathrm{eff}}}\right)^{1/4} H_m\left(\sqrt{\frac{\mathfrak{Re}\ c}{\hbar_{\mathrm{eff}}}}(q-j)\right) \times \exp\left(-\frac{c}{2\hbar_{\mathrm{eff}}}(q-j)^2 + \frac{\mathrm{i}}{4\hbar_{\mathrm{eff}}}(q-j/2)\right) \ , \tag{A8}$$

where H_m is the mth Hermite polynomial. The complex tilting factor $c = (\sqrt{351} - 13\,\mathrm{i})/40$ describes the orientation of the ellipse that can be derived from the linearized map.

Appendix B: Master equation approach for complete flooding

In the extreme case where all regular basis states of the system are completely flooded, we can describe the time-dependent flooding by a master equation. It considers several regular basis states and one chaotic reservoir representing all chaotic basis states. Their weights p^{reg}_m and p^{ch} change due to the tunneling rates $\gamma^{\mathrm{ch}\to\mathrm{reg}}_m$, Eq. (19),

$$\frac{\mathrm{d}}{\mathrm{d}t}p^{\mathrm{reg}}_m(t) = \gamma^{\mathrm{ch}\to\mathrm{reg}}_m p^{\mathrm{ch}}(t) - \gamma^{\mathrm{reg}\to\mathrm{ch}}_m p^{\mathrm{reg}}_m(t) \tag{B1}$$
$$\frac{\mathrm{d}}{\mathrm{d}t}p^{\mathrm{ch}}(t) = \sum_m \left(\gamma^{\mathrm{reg}\to\mathrm{ch}}_m p^{\mathrm{reg}}_m(t) - \gamma^{\mathrm{ch}\to\mathrm{reg}}_m p^{\mathrm{ch}}(t)\right) \tag{B2}$$

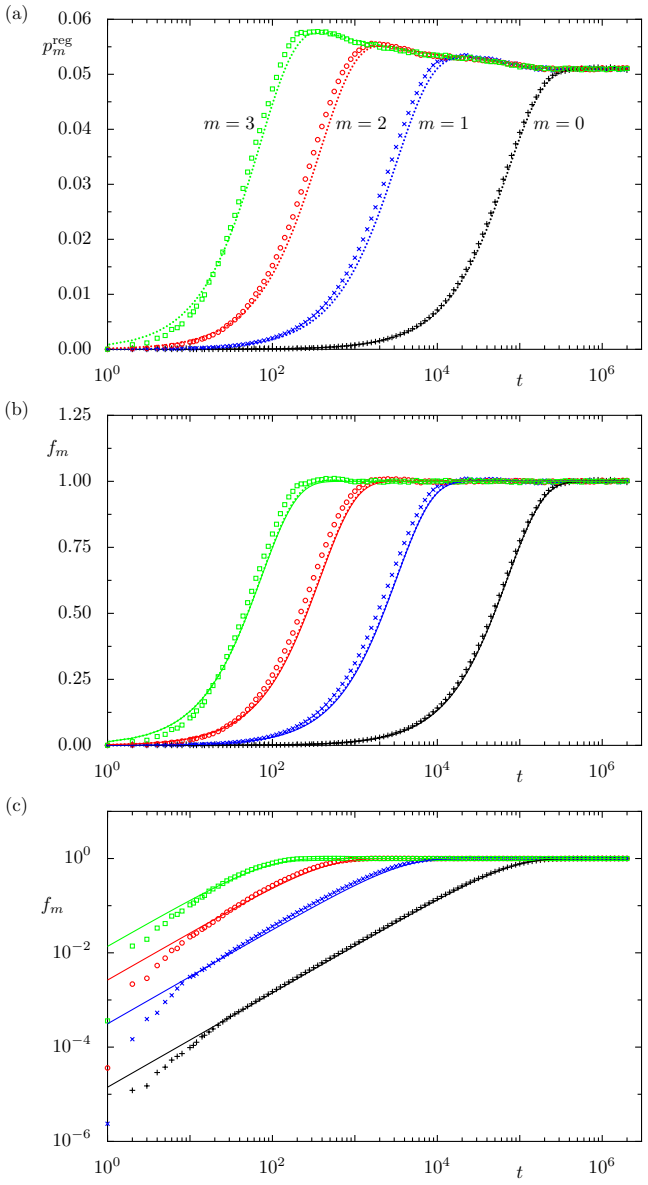

FIG. 11. a) Regular weights $p_m^{\rm reg}(t)$ of the designed map for the case of complete flooding, $N = 3\ 853\ 335, M = 196\ 418, h_{\rm eff} = 1/20$, for $m = 0, 1, 2, 3$ (symbols) compared to Eq. (B5) (dotted lines). b) Corresponding flooding weights $f_m(t)$ and the analytical result of Eq. (50) (solid lines, almost indistinguishable from the dotted lines). c) Double-logarithmic representation of the same data as in b).

Rephrasing these equations in matrix form gives

$$\frac{\rm d}{{\rm d}t}\begin{pmatrix} p_0^{\rm reg}(t) \\ \vdots \\ p_{m_{\rm max}-1}^{\rm reg}(t) \\ p^{\rm ch}(t) \end{pmatrix} = A \begin{pmatrix} p_0^{\rm reg}(0) \\ \vdots \\ p_{m_{\rm max}-1}^{\rm reg}(0) \\ p^{\rm ch}(0) \end{pmatrix} \tag{B3}$$

with

$$A = \begin{pmatrix} -\gamma_0^{\rm reg\to ch} & & 0 & \gamma_0^{\rm ch\to reg} \\ & \ddots & & \vdots \\ 0 & & -\gamma_{m_{\rm max}-1}^{\rm reg\to ch} & \gamma_{m_{\rm max}-1}^{\rm ch\to reg} \\ \gamma_0^{\rm reg\to ch} & \cdots & \gamma_{m_{\rm max}-1}^{\rm reg\to ch} & -\sum_m \gamma_m^{\rm ch\to reg} \end{pmatrix} . \tag{B4}$$

Its solution is given by

$$\begin{pmatrix} p_0^{\rm reg}(t) \\ \vdots \\ p_{m_{\rm max}-1}^{\rm reg}(t) \\ p^{\rm ch}(t) \end{pmatrix} = \exp(At) \begin{pmatrix} p_0^{\rm reg}(0) \\ \vdots \\ p_{m_{\rm max}-1}^{\rm reg}(0) \\ p^{\rm ch}(0) \end{pmatrix} . \tag{B5}$$

For the initial conditions $p^{\rm ch}(0) = 1$ and $p_m^{\rm reg}(0) = 0$ for all m, modeling a wave packet started in the chaotic sea, good agreement with the regular weights obtained for the quantum map is observed, Fig. 11(a). The same also holds for the flooding weights $f_m(t)$, Eq. (13), see Figs. 11(b) and (c). This example nicely demonstrates the advantage of the flooding weights $f_m(t)$ having the same shape for all m, in contrast to the regular weights $p_m^{\rm reg}(t)$.

Considering just the subsystem of one regular state with quantum number m and the chaotic reservoir the matrix A reduces to a 2×2 matrix. This allows for an analytical solution for the regular weight $p_m^{\rm reg}(t)$ from Eq. (B5) and yields Eq. (50) for the flooding weight $f_m(t)$. This analytical result is indistinguishable in Figs. 11(b) and (c) from the solution of the full master equation. It describes the transition from the initial linear increase to saturation in the case of a completely flooded regular torus.

[1] H.-J. Stöckmann, *Quantum Chaos: an introduction*, Cambrige University Press, Cambridge (2000)
[2] F. Haake, *Quantum Signatures of Chaos*, Springer-Verlag, Berlin, 3rd revised and enlarged edition ed. (2010)
[3] I. C. Percival, J. Phys. B **6**, L229 (1973)
[4] M. V. Berry, J. Phys. A **10**, 2083 (1977)
[5] A. Voros, in "Stochastic Behavior in Classical and Quantum Hamiltonian Systems", , edited by G. Casati and J. Ford, Springer-Verlag, Berlin, vol. 93 of *Lect. Notes Phys.*, pp. 326–333 (1979)
[6] O. Bohigas, S. Tomsovic, and D. Ullmo, Phys. Rep. **223**, 43 (1993)
[7] T. Prosen and M. Robnik, J. Phys. A **26**, L319 (1993)
[8] B. Li and M. Robnik, J. Phys. A **28**, 4843 (1995)
[9] G. Carlo, E. Vergini, and A. J. Fendrik, Phys. Rev. E **57**, 5397 (1998)

[10] G. Veble, M. Robnik, and J. Liu, J. Phys. A **32**, 6423 (1999)

[11] A. Bäcker, R. Ketzmerick, S. Löck, and H. Schanz, Europhys. Lett. **94**, 30004 (2011)

[12] R. S. MacKay, J. D. Meiss, and I. C. Percival, Physica D **13**, 55 (1984)

[13] R. C. Brown and R. E. Wyatt, Phys. Rev. Lett. **57**, 1 (1986)

[14] T. Geisel, G. Radons, and J. Rubner, Phys. Rev. Lett. **57**, 2883 (1986)

[15] N. T. Maitra and E. J. Heller, Phys. Rev. E **61**, 3620 (2000)

[16] M. Michler, A. Bäcker, R. Ketzmerick, H.-J. Stöckmann, and S. Tomsovic, Phys. Rev. Lett. **109**, 234101 (2012)

[17] M. J. Davis and E. J. Heller, J. Chem. Phys. **75**, 246 (1981)

[18] S. Keshavamurthy and P. Schlagheck, *Dynamical Tunneling: Theory and Experiment*, Taylor & Francis (2011)

[19] A. Bäcker, R. Ketzmerick, and A. G. Monastra, Phys. Rev. Lett. **94**, 054102 (2005)

[20] A. Bäcker, R. Ketzmerick, and A. G. Monastra, Phys. Rev. E **75**, 066204 (2007)

[21] J. Feist, A. Bäcker, R. Ketzmerick, S. Rotter, B. Huckestein, and J. Burgdörfer, Phys. Rev. Lett. **97**, 116804 (2006)

[22] J. Feist, A. Bäcker, R. Ketzmerick, J. Burgdörfer, and S. Rotter, Phys. Rev. B **80**, 245322 (2009)

[23] A. Ishikawa, A. Tanaka, and A. Shudo, Phys. Rev. Lett. **104**, 224102 (2010)

[24] S. Löck, A. Bäcker, R. Ketzmerick, and P. Schlagheck, Phys. Rev. Lett. **104**, 114101 (2010)

[25] N. Mertig, S. Löck, A. Bäcker, R. Ketzmerick, and A. Shudo, Europhys. Lett. **102**, 10005 (2013)

[26] A. Bäcker, R. Ketzmerick, S. Löck, and N. Mertig, Phys. Rev. Lett. **106**, 024101 (2011)

[27] A. Bäcker, R. Ketzmerick, S. Löck, J. Wiersig, and M. Hentschel, Phys. Rev. A **79**, 063804 (2009)

[28] S. Löck, A. Bäcker, and R. Ketzmerick, Phys. Rev. E **85**, 016210 (2012)

[29] L. Hufnagel, R. Ketzmerick, M.-F. Otto, and H. Schanz, Phys. Rev. Lett. **89**, 154101 (2002)

[30] M. V. Berry, N. L. Balazs, M. Tabor, and A. Voros, Ann. Phys. **122**, 26 (1979)

[31] J. H. Hannay and M. V. Berry, Physica D **1**, 267 (1980)

[32] S.-J. Chang and K.-J. Shi, Phys. Rev. A **34**, 7 (1986)

[33] M. Degli Esposti, Ann. Inst. H. Poincaré Phys. Théor. **58**, 323 (1993)

[34] L. Bittrich, Dissertation, Technische Universität Dresden, Fachrichtung Physik (2010)

[35] A. Bäcker, R. Ketzmerick, and S. Löck, Phys. Rev. E **82**, 056208 (2010)

[36] A. Bäcker, R. Ketzmerick, S. Löck, and L. Schilling, Phys. Rev. Lett. **100**, 104101 (2008)

[37] F. Leyvraz and D. Ullmo, J. Phys. A **29**, 2529 (1996)

[38] J. Zakrzewski, D. Delande, and A. Buchleitner, Phys. Rev. E **57**, 1458 (1998)

[39] S. Tomsovic and D. Ullmo, Phys. Rev. E **50**, 145 (1994)

[40] L. Schilling, Dissertation, Institut für Theoretische Physik, Fachrichtung Physik, Fakultät Mathematik und Naturwissenschaften, Technische Universität Dresden (2006)

[41] F. Mezzadri, Not. Am. Math. Soc. **54**, 592 (2007)

[42] D. Adams, *The Hitchhiker's Guide to the Galaxy: the Trilogy of Four*, Picador, London (2002)

[43] B. V. Chirikov, Phys. Rep. **52**, 263 (1979)

[44] L. A. Bunimovich, Chaos **11**, 802 (2001)

[45] T. Betcke and L. N. Trefethen, SIAM Review **47**, 469 (2005)

[46] T. Betcke, SIAM J. Sci. Comput. **30**, 1278 (2008)

[47] A. Bäcker, R. Ketzmerick, S. Löck, M. Robnik, G. Vidmar, R. Höhmann, U. Kuhl, and H.-J. Stöckmann, Phys. Rev. Lett. **100**, 174103 (2008)

[48] L. Bittrich, A. Bäcker, R. Ketzmerick, U. Kuhl, and H.-J. Stöckmann, "Reappearance of flooded regular states in open quantum systems", in preparation